Interaction of Monotopic Membrane Enzymes with a Lipid Bilayer: A Coarse-Grained MD Simulation Study[†]

Kia Balali-Mood, Peter J. Bond,[‡] and Mark S. P. Sansom*

Department of Biochemistry, University of Oxford, South Parks Road, Oxford OX1 3QU, U.K.

Received September 11, 2008; Revised Manuscript Received January 21, 2009

ABSTRACT: Monotopic membrane proteins bind tightly to cell membranes but do not generally span the lipid bilayer. Their interactions with lipid bilayers may be studied via coarse-grained molecular dynamics (CG-MD) simulations. Understanding such interactions is important as monotopic enzymes frequently act on hydrophobic substrates, while X-ray structures rarely provide direct information about their interactions with membranes. CG-MD self-assembly simulations enable prediction of the orientation and depth of insertion into a lipid bilayer of a monotopic protein, and also of the interactions of individual protein residues with lipid molecules. The CG-MD method has been evaluated via comparison with extended (>30 ns) atomistic simulations of monoamine oxidase, revealing good agreement between the results of coarse-grained and atomistic simulations. CG-MD simulations have been applied to a set of 11 monotopic proteins for which three-dimensional structures are available. These proteins may be divided into two groups on the basis of the results of the simulations. One group consists of those proteins which are inserted into the lipid bilayer to a limited extent, interacting mainly at the phospholipid−water interface. The second group consists of those which are inserted more deeply into the bilayer. Those monotopic proteins which are inserted more deeply cause significant local perturbation of bilayer properties such as bilayer thickness. Deeper insertion seems to correlate with a greater number of basic residues in the "foot" whereby a monotopic protein interacts with the membrane.

Membranes play a key role in the biology of cells. It is well established that integral membrane proteins account for more than 20% of genes (*1*). Despite a slow start, structural biology studies of integral membrane proteins are making steady progress (*2*), accompanied by advances in structural bioinformatics (*3*). However, there is another important class of membrane proteins, namely the monotopic membrane proteins (*4*). These proteins bind tightly to the membrane, often penetrating the hydrophobic core; however, they do not generally span the lipid bilayer, and the majority of the protein mass lies outside the membrane. There have been some preliminary structural bioinformatics studies of monotopic membrane proteins (*3*), but the nature of their interactions with the bilayer surface (or more properly at the bilayer−water interface) is less well characterized than the interactions of integral membrane proteins with lipids (*5, 6*). Given many monotopic membrane proteins are enzymes of some importance as pharmacological targets (*4, 7*) acting on hydrophobic substrates, it is important that an improved understanding of the nature of their interactions with lipid bilayers is developed.

A number of high-resolution X-ray structures of monotopic enzymes and related proteins have been determined (Table 1). In addition to the protein structures, we need to understand both the location of a monotopic protein relative to the membrane and the nature of its interactions with lipids. Although structural biology can provide some information about, for example, bound lipid molecules (*5*), most crystal structures do *not* include an intact bilayer. In this respect, computer simulations are a valuable tool, enabling us to study the dynamic interactions of membrane proteins with lipids (reviewed in, e.g., ref *8*). There have been a number of atomistic simulation studies of the interactions of selected monotopic proteins with membranes (*9*−*11*), although these have been somewhat restricted by the duration of the simulations (typically ∼10 ns or less) which result in incomplete sampling of protein−lipid interactions. A number of other computational approaches have been developed which enable prediction of the membrane localization of monotopic proteins (*12*−*15*). However, these treat the bilayer

Table 1: Monotopic Enzymes Examined in This Study[a]

protein	PDB entry	resolution (Å)	no. of residues	oligomer	ref
11-β HSD	1XSE	2.5	297	monomer	*57*
ACO	2BIX	2.7	490	monomer	*40*
COX-1	1Q4G	2.0	553	dimer	*58*
COX-2	1CVU	2.4	552	dimer	*42*
CrAT	1T7Q	1.8	625	monomer	*59*
ETF-QO	2GMH	2.5	584	monomer	*38*
FAAH	1MT5	2.8	537	dimer	*37*
MAO-B	1OJA	2.0	520	dimer	*60*
OSC	1W6K	2.1	732	monomer	*36*
P450	2BDM	2.3	492	monomer	*41*
SHC	2SQC	2.0	630	dimer	*43*

[a] Seven (11-β HSD, ACO, COX-1, COX-2, ETF-QO, MAO-B, and P450) of the enzymes are oxidoreductases. Two (OSC and SHC) are isomerases. CrAT is a transferase. FAAH is a hydrolase.

[†] This work was funded by the BBSRC and EPSRC.

* To whom correspondence should be addressed. E-mail: mark.sansom@bioch.ox.ac.uk. Telephone: +44-1865-613306. Fax: +44-1865-613238.

[‡] Current address: Max Planck Institute of Biophysics, Max-von-Laue-Str. 3, 60438 Frankfurt/Main, Germany.

10.1021/bi8017398 CCC: $40.75
Published on Web 01/22/2009

as a hydrophobic slab of constant thickness and so omit both protein−headgroup interactions and bilayer deformability.

A more recent approach to membrane protein simulations is the use of coarse-grained simulations, initially developed for lipids (*16, 17*) and more recently extended to integral membrane proteins (see, e.g., refs *6* and *18*−*20*, with a more extensive review in ref *8*). Coarse-grained molecular dynamics (CG-MD)[1] simulations may also be used to predict the interactions of proteins with the lipid bilayer surface. This has been evaluated for small protein toxins (*21*) and for "simple" peripheral membrane proteins (e.g., PLA_2) (*22*) for which experimental biophysical data are available. Here we apply the CG-MD approach to a set of 11 monotopic membrane protein enzymes. We show that the predominant interactions are via basic residues with lipid headgroups alongside hydrophobic interactions with the bilayer core. Furthermore, a number of monotopic proteins are suggested to be able to perturb the bilayer structure local to the protein, which may be of functional significance.

METHODS

Protein Preparation. Structures of 11 monotopic proteins (see Table 1) were selected from the Protein Data Bank and downloaded. When multiple structures were present for a given protein, higher-resolution structures were selected. Missing side chain atoms were modeled using InsightII followed by a short (100 step) cycle of energy minimization to alleviate any bad contacts. The resultant atomistic structures were stripped of all non-protein atoms and converted into a coarse-grained model as described previously (*6, 19, 23*).

Coarse-Grained Molecular Dynamics Simulations. All CG simulations were performed using GROMACS version 3.1.4 (*24*) using the CG model of Marrink and colleagues (*16*) extended for use with membrane proteins and peptides (*6, 19, 23*). In this CG model, each amino acid is represented by one backbone particle, whose Cartesian coordinates correspond to that of the Cα atom, and between one and three side chain particle(s) depending on the residue size. The secondary and tertiary structures of the protein are modeled as an elastic network model (ENM) (*25*) by imposing a harmonic restraint (force constant of 10 kJ mol^{-1} $Å^{-2}$) between all backbone particles that were within 7 Å of each other. The Cα root-mean-square deviation of the proteins from the initial structure did not exceed ∼3 Å in any of the simulations performed.

A time step of 40 fs was used in all CG-MD simulations, with coordinates saved every 100 ps for subsequent analysis. Periodic boundary conditions were employed, and the Berendsen (*26*) temperature and pressure coupling algorithms were used with a time constant of 1 ps for both. Anisotropic pressure coupling was used, with the same compressibility (4×10^{-5}) in all directions. Lennard-Jones interactions were shifted to zero between 0.9 and 1.2 nm, and electrostatics were shifted to zero between 0 to 1.2 nm, with a relative dielectric constant of 20.

Table 2: Summary of Simulations[a]

protein	no. of DPPCs	protein contacts to DPPC[b] (%)	hydrophobic contact fraction[c] (%)	basic contact fraction[c] (%)	insertion depth[d] (Å)
11-β HSD	320 or 640	34 (3)	53 (2)	30 (1)	11 (2)
ACO	320 or 640	12 (2)	39 (2)	17 (1)	24 (1)
COX-1	320 or 640	23 (2)	46 (3)	26 (1)	18 (2)
COX-2	320 or 640	28 (3)	52 (3)	28 (0.4)	17 (2)
CrAT	320 or 640	16 (3)	52 (3)	21 (0.5)	23 (1)
ETF-QO	320 or 640	9 (3)	50 (3)	21 (1)	22 (1)
FAAH	320 or 640	20 (3)	46 (3)	17 (1)	27 (1)
MAO-B	320 or 640	17 (3)	52 (3)	17 (1)	10 (0.3)
OSC	256 or 512	16 (3)	45 (3)	17 (1)	23 (1)
P450	320 or 640	21 (2)	41 (2)	19 (1)	23 (1)
SHC	320 or 640	26 (2)	49 (2)	28 (0.5)	17 (1)

[a] For each protein, five simulations were performed: three with the smaller number of lipid molecules (i.e., 256 or 320 DPPCs) and two with the larger (512 or 640) number of lipids. All simulations were run for 700 ns. The number of water particles present varied from ∼6000 to ∼8000 for the smaller simulations and from ∼11000 to ∼15000 for the larger simulations. [b] The protein contacts are the number of contact residues as a percentage of the total number of residues in a given protein. These contacts were calculated as averages (standard deviation) for the larger bilayer systems between 100 and 700 ns, using an interparticle cutoff of 8 Å (corresponding approximately to two CG particles in contact with one another). [c] The hydrophobic and basic contact fractions are the percentage of residues forming contacts which are either hydrophobic or basic. [d] The insertion depth was calculated as the vertical (i.e., *z*) distance between the center of mass of the membrane binding domain of the protein and of the lipid bilayer.

Proteins were "inserted" into bilayers by self-assembly simulations, in which a bilayer is allowed to form from randomly positioned and oriented lipid and water molecules in the presence of the protein (*6*). Five simulations were run for each protein: three with a smaller number of lipid molecules (i.e., 256 or 320) and two with a larger (512 or 640) number (see Table 2). In each simulation, the protein was placed in the center of a simulation box. Phospholipid [dipalmitoylphosphatidylcholine (DPPC)] molecules were then added at random positions and orientations within the simulation box. The system was hydrated with CG water particles and then energy-minimized, using the steepest-descent algorithm, prior to simulation. The duration of each simulation was 700 ns.

Atomistic Molecular Dynamics Simulations. Atomistic simulations of MAO-B (see below) were performed as described in detail in ref *11*. The simulation analyzed in this study is an extension (to >30 ns) of the 15 ns simulation presented in this earlier study. MAO-B was inserted into a preformed and equilibrated bilayer made up of 478 palmitoyloleoylphosphatidylethanolamine (POPE) and 654 palmitoyloleoylphosphatidylcholine (POPC) molecules. Simulations used the GROMOS96 (*27*) force field. Long-range electrostatic forces were calculated using the particle mesh Ewald method (*28*), and van der Waals interactions were computed for all pairs of atoms separated by no more than 10 Å. The lengths of all bonds were constrained using the LINCS algorithm (*29*), permitting an integration time step of 2 fs to be used. The protein was simulated in the isobaric−isothermal ensemble, and a constant pressure of 1

[1] Abbreviations: 11-β HSD, 11-β-hydroxysteroid dehydrogenase; ACO, apocarotenoid cleavage oxygenase; AT-MD, atomistic molecular dynamics; CG-MD, coarse-grained molecular dynamics; COX-1, cyclooxygenase 1 (prostaglandin H2 synthase 1); COX-2, cyclooxygenase 2 (prostaglandin H2 synthase 2); CrAT, carnitine acyltransferase; DPPC, dipalmitoylphosphatidylcholine; ENM, elastic network model; ETF-QO, electron transfer flavoprotein-ubiquinone oxidoreductase; FAAH, fatty acid amide hydrolase; MAO-B, monoamine oxidase B; OSC, oxidosqualene cyclase; PLA_2, phospholipase A_2; POPC, palmitoyloleoylphosphatidylcholine; POPE, palmitoyloleoylphosphatidylethanolamine; rmsd, root-mean-square deviation; rmsf, root-mean-square fluctuation; SHC, squalene hopene cyclase.

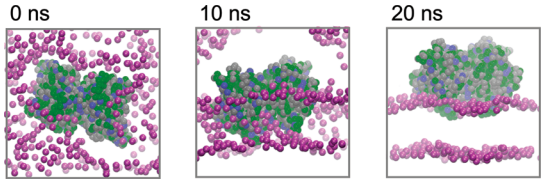

FIGURE 1: CG bilayer self-assembly around the FAAH dimer. Purple spheres represent the phosphate headgroup particles of the DPPC molecules. The protein is in van der Waals representation with green for hydrophobic residues, blue for basic residues, and gray for all other residues. This and other figures were prepared using VMD (*32*).

bar was applied independently in all directions using a Parrinello-Rahman barostat (*30*) using a pressure coupling constant of 5.0 ps. Water, lipid, and protein were coupled separately to Nosé-Hoover thermostats at 300 K with a temperature coupling constant of 1.0 ps (*31*). All analysis of the MD trajectories was performed using either the GROMACS suite of analysis programs or VMD (*32*).

RESULTS

Coarse-Grained Self-Assembly Simulations. CG-MD simulations were performed in which the lipid bilayer is allowed to self-assemble in the presence of the known structure of the monotopic membrane protein (illustrated for FAAH in Figure 1). It can be seen that the bilayer self-assembles around the protein within ~20 ns. This has also been seen for CG-MD self-assembly simulations of *integral* membrane proteins (*6*). All simulations were therefore performed for 700 ns and analysis of, e.g., protein−lipid interactions performed over the period of 100−700 ns to ensure that the system had equilibrated prior to analysis.

Previous studies of integral membrane proteins and peptides (*19, 23*) have shown that it will reproduce experimental data for membrane-spanning proteins. These studies include simulations of the location (transmembrane vs surface) of α-helical peptides for which there are solid state NMR and other spectroscopic data (*19, 23*) and self-assembly of the glycophorin A transmembrane helix dimer (*33*), the structure of which has been determined by NMR. Simulations of a small protein toxin (*21*) and of the secreted membrane active enzyme phospholipase A_2 (*22*) have demonstrated the validity of the methodology for proteins which bind to the lipid−water interface, and that the self-assembly procedure yields results similar to those found when the protein is allowed to interact with a preformed lipid bilayer. For larger, more complex, monotopic proteins, we selected the self-assembly procedure described above as it allows for the possibility of a greater potential degree of insertion of the protein into the bilayer. As a control, we chose a globular protein similar in size to the set of monotopic proteins studied, namely the globular head of the complement system protein C1q [Protein Data Bank entry 1PK6 (*34*)]. Three repeat self-assembly simulations yielded no association of this protein with the bilayer, confirming the ability of the CG-MD self-assembly procedure to distinguish between globular proteins and monotopic membrane proteins.

Comparison with Atomistic Simulations. To evaluate the accuracy of CG-MD simulations of membrane-bound monotopic proteins, we compared an atomistic (AT-MD; 32 ns duration) simulation (an extension of that discussed in ref

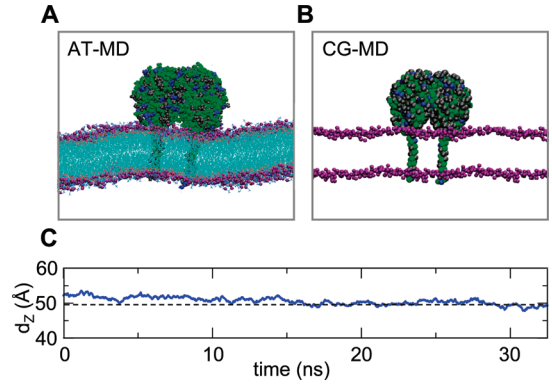

FIGURE 2: Comparison of (A) atomistic [AT-MD; at 15 ns (*11*)] and (B) coarse-grained (CG-MD; at 700 ns) simulations of membrane-bound MAO-B. In the AT-MD simulation, the lipids are POPE and POPC (3:4 ratio); in the CG-MD simulation, they are DPPC. The color scheme is as follows. For the lipids, phosphates are colored purple and lipid tails (AT-MD only) cyan. For the protein, basic residues are colored blue, hydrophobic residues green, and others gray. (C) Distance, along the bilayer normal, between the protein and bilayer centers of mass for the AT-MD simulation of MAO-B. The broken horizontal line corresponds to the equilibrium location of MAO-B, estimated from the latter half of the simulation.

11) and a CG-MD simulation of the dimeric form of membrane-bound MAO-B (Figure 2). In the AT-MD simulation, the initial position was derived from consideration of the TM helix anchors (see the discussion in ref *11*). Analysis of the distance between the protein and bilayer centers of mass for the AT-MD simulation (Figure 2C) indicates that after the first 10 ns or so, the protein has reached an equilibrium position relative to the bilayer. Furthermore, the Cα root-mean-square deviation (rmsd; fitted onto the $t = 0$ structure) reached a value of ~2 Å after 20 ns and remained stable, for each monomer. We also extended the hydrogen bond analysis of our earlier 15 ns simulation (*11*) and observed no substantial change, such that after ~20 ns the hydrogen bonding pattern stabilizes at a level between seven and nine hydrogen bonds between the membrane binding domain of the protein and the phospholipids. Thus, the extended AT-MD simulation may be used to evaluate the CG-MD simulations, for which the self-assembly protocol was used.

In terms of the location in the bilayer, both CG-MD self-assembly simulations gave results very similar to those of the AT-MD simulations (Figure 3). We ran our CG-MD simulations both with a single lipid species (DPPC) and with a mixed lipid bilayer (POPE/POPC), in the latter case using the same lipid ratio (3:4) as in the AT-MD simulation. In all three cases, the TM helix anchors span the bilayer while the bulk of protein is outside the membrane, with a degree of overlap of the protein (residues Y97:A, W107:A, W157:A, F481:A, H485:A, F481:B, H485:B, and R494:B) with the headgroups and with the outer region of the hydrophobic tails of the upper leaflet of the bilayer. The headgroup−headgroup thickness of the bilayer was ~35 Å for both the AT-MD and CG-MD simulations. [Please note this is smaller than the phosphate−phosphate distance (see below) as the "headgroup" was defined to include the glycerol moiety.] Interestingly, we observe no difference between the bilayer orientation of MAO-B in DPPC bilayers versus POPC/POPE bilayers in our CG-MD simulations.

In the CG-MD simulations, the tertiary structure of the protein is maintained by an elastic network model (see, e.g.,

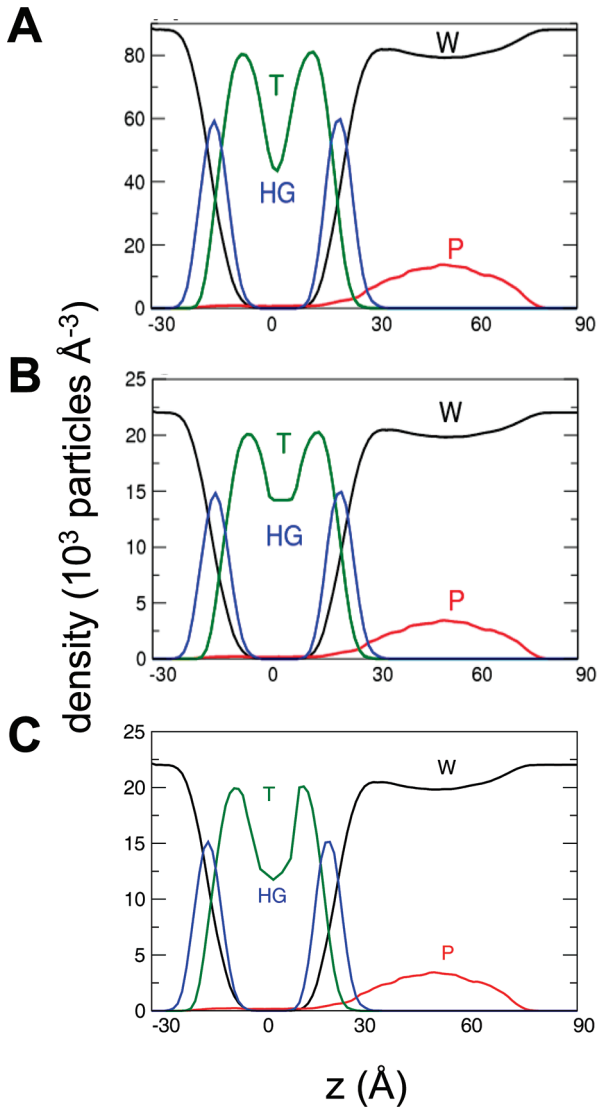

FIGURE 3: Partial density profiles of the atomistic (A) and coarse-grained (B and C) MAO-B systems. In the AT-MD simulation, the lipids are POPE and POPC (3:4); in the CG-MD simulations, they are (B) DPPC or (C) POPE and POPC (3:4). The black line represents the distribution of water (W). The red line displays the distribution of the protein (P). The green line is representative of the lipid tails (T). The two blue lines represent the headgroups (HG) in each leaflet of the bilayer.

refs *25* and *35*). The effectiveness of this in maintaining the overall local dynamics of the protein may be evaluated by comparison of the Cα atom root-mean-square fluctuation (rmsf) profiles for the AT-MD and CG-MD simulations (Figure 4). The two profiles are very similar, which has been seen in other analyses of ENMs (*25, 35*). The values for the CG system are perhaps slightly elevated, which may reflect the smoothing of the energy landscape of the protein which results in slightly less restrained Cα motions (the "Cα" particles of the CG model representing all backbone atoms of the AT structure).

A more qualitative comparative measure between the CG and AT simulations is provided by the (time-averaged) protein lipid contacts. Visual inspection of those residues forming the most frequent contacts in the CG versus AT simulations shows that the residues primarily involved in the protein−lipid contacts were a combination of basic (e.g., K93:A, K154:B, and R484:B) and hydrophobic residues (e.g., F119:A and L139:B) in both cases. These residues are located in the main membrane surface binding domain of the protein, not the transmembrane helices. We do however see more contacts in the transmembrane helices of MAO-B in the CG system. This may reflect the greater sampling of lipid configurations in the CG (700 ns) versus the atomistic (∼30 ns) simulations.

Overall, this comparison suggests the CG methodology can be used with some confidence in the analysis of the interactions of monotopic membrane enzymes. We therefore proceeded to CG-MD simulations of a wider range of such enzymes.

CG-MD of Monotopic Membrane Enzymes. Having evaluated the CG-MD approach for self-assembly of monotopic protein bilayer systems, we have used it to survey systematically a set of 11 monotopic proteins (Table 1). These range in size from 11-β HSD (11-β-hydroxysteroid dehydrogenase) to SHC (squalene hopene cyclase). All of these proteins have been suggested to bind to the membrane surface or interface.

For each protein, five simulations were performed: three with a smaller bilayer and two with a larger bilayer (see Table 2 for details). Snapshots of the final configurations from some of these simulations are shown in Figure 5. Preliminary examination suggests that while some proteins (e.g., FAAH) cause minimal perturbation to the bilayer in the vicinity of their attachment, others (e.g., COX-2) result in significant local bilayer perturbation.

This difference may be probed further via analysis of partial density profiles for the lipid and protein components along the bilayer normal. For this purpose, each protein density profile was divided into three amino acid groupings: hydrophobic, basic, and other. The phospholipids in the bilayer were also analyzed as headgroup and tail regions, respectively. From this analysis (Figure 6), one can see that the proteins fall into two main classes. Most (i.e., ACO, FAAH, P450, OSC, and CrAT) do not insert deeply into the bilayer. Rather, they interact with only the lipids of the upper leaflet (i.e., the one on the same side of the bilayer as the protein) and do not insert substantially beyond the headgroup region of this leaflet. The other category (i.e., COX-1, COX-2, 11-β HSD, and SHC) consists of those proteins which insert more deeply into the bilayer and/or lead to a local deformation of the bilayer. In all of the latter cases, some of the protein residues can be seen to insert beyond the upper headgroup region into the hydrophobic core of the bilayer.

We observed asymmetric insertion of COX-1 deep into a bilayer. We demonstrated that this was not evidence of a lack of convergence and/or a local minimum of the simulation, as the simulation was repeated three times with 320 lipids and two times with 640 lipids (Table 2), yielding substantially the same result. A similar behavior is seen for the closely related protein COX-2. However, as COX-2 contains more basic residues than COX-1 in the "foot" region, it interacts and/or binds with headgroups in the opposite leaflet to a far greater extent than COX-1. This interaction with lipids (in particular phosphate groups) leads to significant thinning (see below) and subsequent curvature of the bilayer. The key residues interacting with the opposing leaflet are basic residues, mainly K and R.

COX-2 appears to cause a greater degree of local bilayer distortion than COX-1. A detailed visual comparison of the

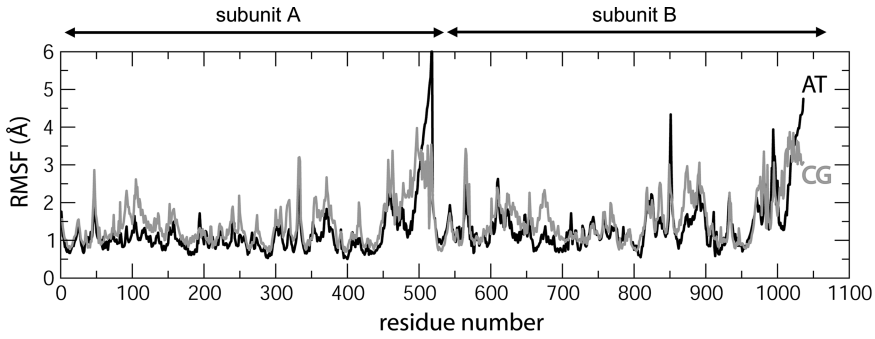

FIGURE 4: Comparison of the Cα atom root-mean-square fluctuation (rmsf) as a function of residue number for the AT-MD (black line) and CG-MD (gray line) simulations of the membrane-bound MAO-B system.

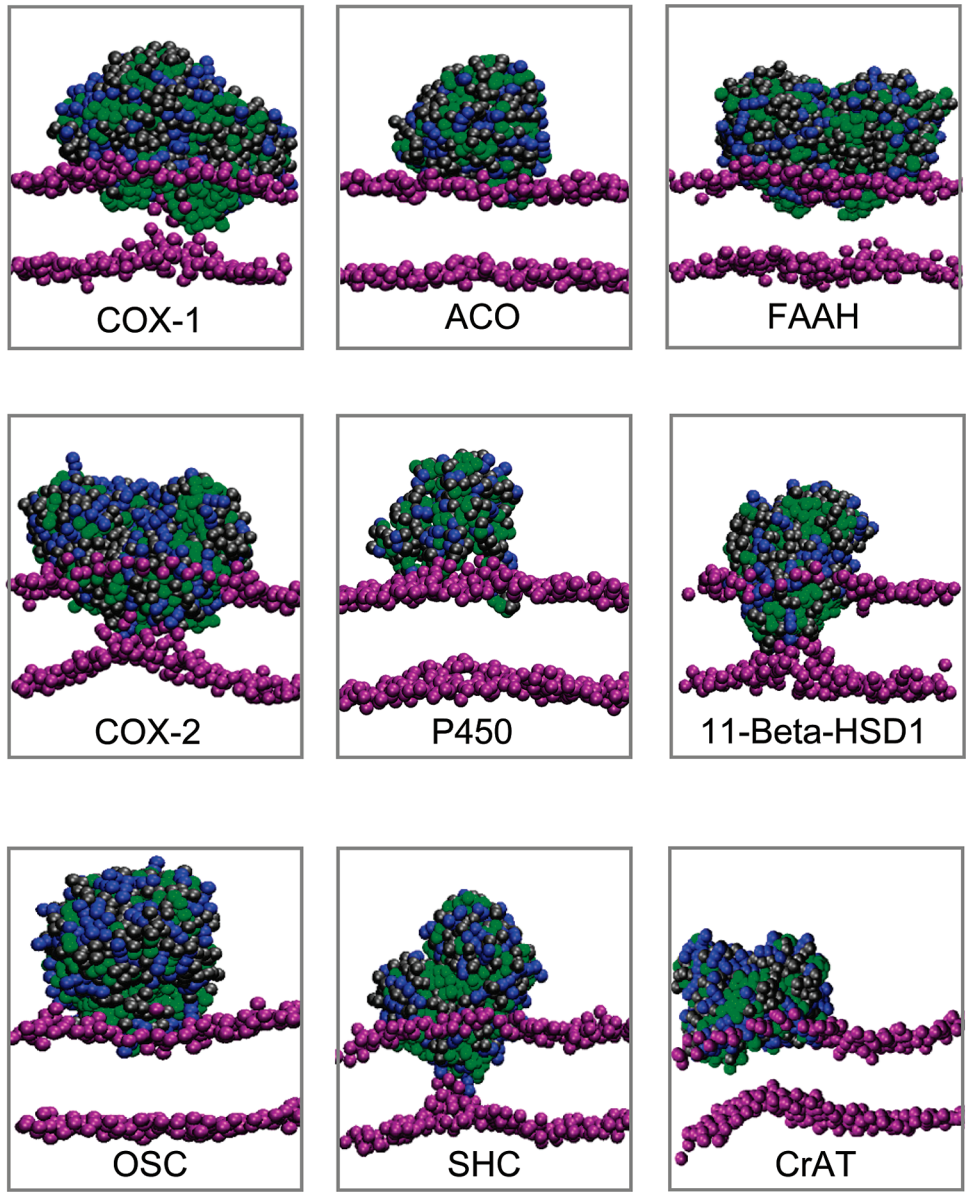

FIGURE 5: Final (t = 700 ns) snapshots of nine membrane-bound monotopic protein bilayers as generated by CG-MD. The color scheme is as in Figure 2, i.e., purple spheres for phosphates and proteins colored green (hydrophobic residues), blue (basic residues), and gray (others).

membrane interaction of COX-1 and COX-2 (Figure 7A,B) shows that both proteins perturb the bilayer by hydrophobic residues penetrating the bilayer center alongside interaction of basic residues with phosphates of the opposing bilayer leaflet. This latter interaction with phosphates of the opposing leaflet may be responsible for the local curvature observed in the bilayer.

Examples of proteins that do not perturb or disrupt the bilayer are provided by OSC and FAAH. These two proteins are oriented in a similar manner. The amphipathic helix of

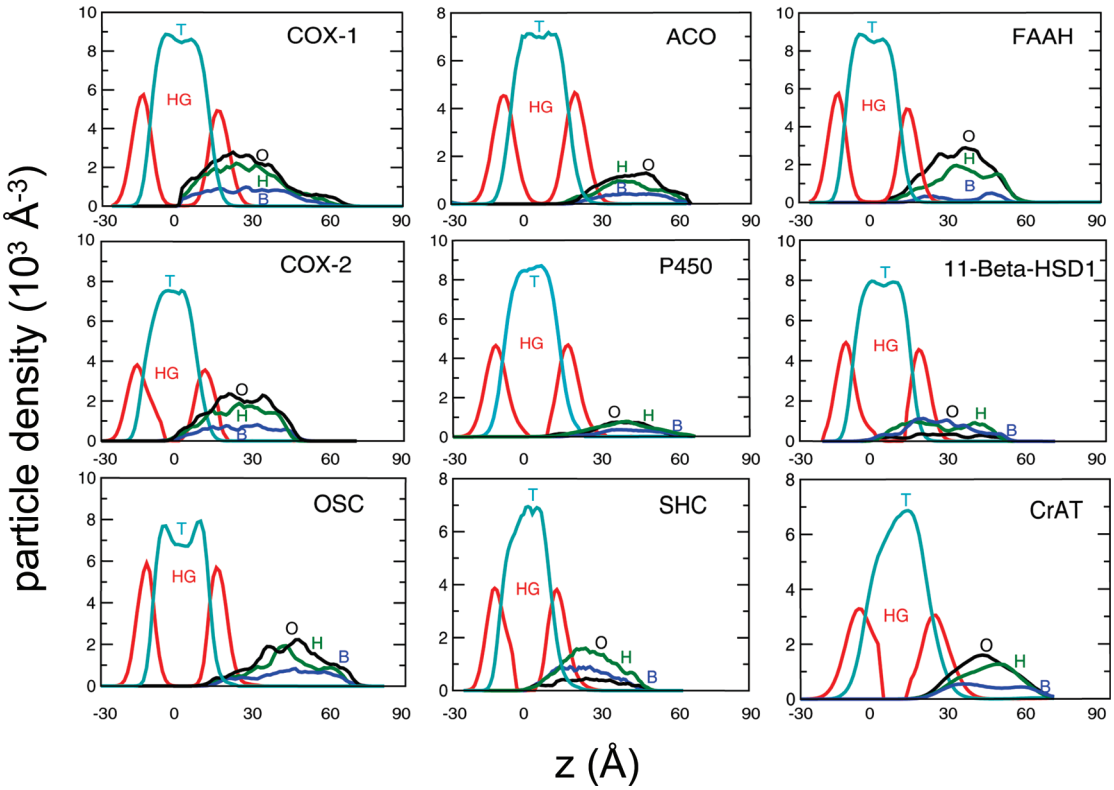

FIGURE 6: Comparison of the distribution of components in nine of the membrane-bound monotopic protein systems. The green line represents the hydrophobic (H) residues of each protein, the blue line the basic (B) residues of each protein, and the black line all other (O) residues of the protein. The two red lines represent the distribution of lipid headgroups. The phospholipid tails are represented by the cyan line.

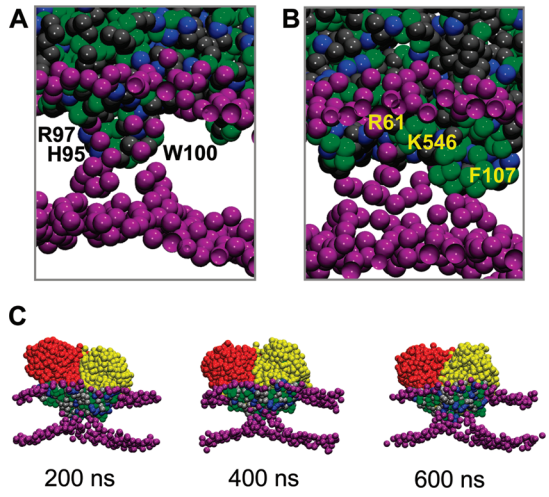

FIGURE 7: Close-up view of the bilayer perturbation by (A) COX-1 and (B) COX-2, in both cases with selected basic and hydrophobic residues labeled. Phosphates are colored purple, and proteins are colored blue (basic residues), green (hydrophobic residues), and gray (all other residues). (C) Snapshots from a simulation of the COX-2 dimer, at 200, 400, and 600 ns, illustrating the rocking motion of the dimer relative to the bilayer. The residues interacting with lipids are colored blue (basic side chains) or green (hydrophobic side chains), while those residues not interacting with lipids are colored red or yellow according to the protein subunit to which they belong.

OSC stabilizes this monomeric protein in the headgroup region as predicted (*36*), some hydrophobic residues of which interact with the acyl chains. FAAH (another monotopic protein that possesses a hydrophobic foot) also does not insert deeply into the bilayer. Rather, FAAH is preferentially located at the headgroup region of the bilayer, with the hydrophobic face of the amphipathic helices protruding into the palmitoyl chains. The bilayer insertion of ACO is less pronounced than for the other monotopic enzymes.

Motion Relative to the Bilayer. As noted above, we observe an asymmetric interaction of a number of dimeric proteins (e.g., COX-1 and COX-2) with the bilayer. However, this is not seen for all dimeric monotopic proteins. Thus, e.g., FAAH (which inserts to a limited extent) seems to interact symmetrically with the bilayer (see Figures 1 and 5), whereas, e.g., COX-2, which inserts more deeply, interacts in an asymmetric fashion. Examination of successive snapshots from the COX-2 simulation (Figure 7C) shows that the degree of asymmetry fluctuates with respect to time and that the dimeric protein appears to "rock" in the bilayer. This appears to correlate with the greater extent of bilayer insertion and consequent local bilayer perturbation (see below) by COX-2.

Key Residues for Protein−Lipid Interactions. It is convenient to divide the proteins investigated into two groups, those which exhibit relatively shallow insertion into the hydrophobic core of the bilayer (FAAH, ACO, P450, ETF-QO, and OSC) and those which exhibit deeper insertion (COX, 11-β HSD1, and CrAT) in some cases interacting with the more distant leaflet of the bilayer. Analysis of those residues which form the most frequent contacts with lipids during the simulations (see Figure 8 for two examples and the Supporting Information for a complete list) provides an indication of the types of residues interacting with the lipids and allows comparison with available experimental data and suggested lipid binding motifs.

Shallow Insertion. (i) FAAH. On the basis of the structure of FAAH (*37*), it has been suggested that this dimeric protein interacts with the membrane by the 16-residue amphipathic

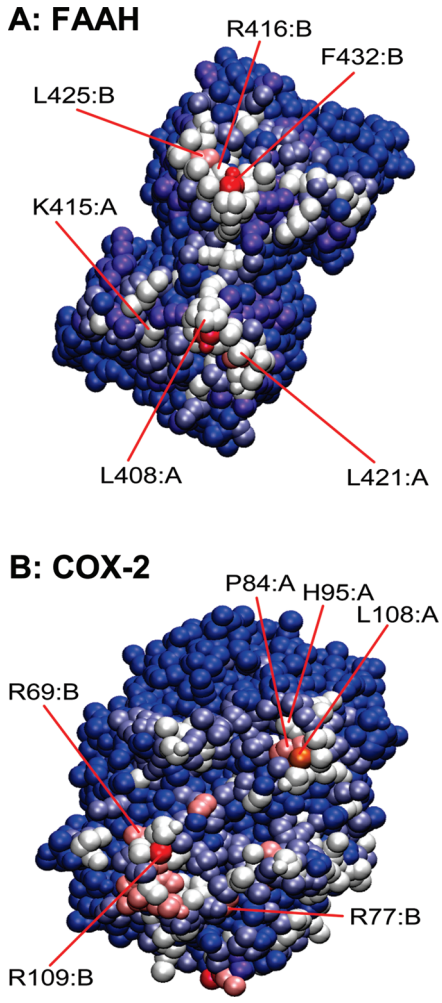

FIGURE 8: Protein−lipid contacts (defined using a cutoff distance of 8 Å; see Table 2 for details), shown on a BWR color scale (blue for no contacts and red for the greatest number of contacts). The view in each case is from the membrane midplane "up" the bilayer normal toward the protein contact: (A) FAAH and (B) COX-2.

helix of each monomer that provides an anchor for insertion into the membrane. In the simulations, we observed interactions of leucines, tryptophans, and phenylalanines (in the amphipathic helices) in the docking of the protein into the bilayer. The main (as judged in terms of frequency of contacts summed over all simulations) hydrophobic residues forming contacts are L408:A, W413:A, F414:A, L417:A, L421:A, and L422:A in subunit A and W413:B, L417:B, L422:B, L425:B, F426:B, and F432:B in subunit B. We also observed basic residues from the helices interacting with the phosphate groups of the lipids, namely, R409:A and K415:A in one subunit and R416:B and K423:B in the other subunit. The membrane binding region other than the amphipathic helix also contained basic residues involved in protein−lipid interactions: R38:A, K423:A, K446:A, H449:A, and R386:B. Overall, the contacts seen in the FAAH simulations seem to be in agreement with the proposed mode of membrane association previously suggested (*37*).

(ii) ETF-QO. On the basis of the structure of electron transfer flavoprotein-ubiquinone oxidoreductase (ETF-QO) (*38*), it is suggested that this protein associates with the bilayer via an amphipathic helix (much like FAAH or COX-1 and -2). A β-sheet region, near the membrane-bound helix, contained a number of basic residues (R116, R271, and H272) suggested to interact strongly with the phophate moieties (*38*). However, in our simulations, these proposed residues did not interact with lipids as frequently as some others, e.g., K22, F274, K281, K288, and D291. In particular, helix 6 (residues 271−291) formed frequent interactions with the phospholipids in our simulations.

(iii) OSC. OSC is believed to interact with the bilayer via a membrane binding domain consisting of three α-helices (*39*). The main residues involved in the interaction of OSC with the bilayer in the simulations were D169, D172, V174, A176, I179, H181, and K183, all of which were located on helix 1. The second helix in the membrane binding domain is buried deeper than helix 1, so we observe a greater number of contacts between phospholipids (acyl chains) and hydrophobic residues. Not surprisingly, we observe that the basic residues predominantly interact with the headgroup region of the bilayer, in particular the charged phosphate moieties. The third helix complements the hydrophobic and electrostatic interactions of the first two helices. The key residues in the third helix were P189, K194, and F195. Overall, the results obtained from our simulations support the proposed binding of OSC (*39*) to the bilayer.

(iv) ACO. The interactions of ACO with the bilayer seen in the simulations agree with those proposed on the basis of the structure (*40*), consisting of a hydrophobic patch consisting mainly of leucines and phenylalanines. The key hydrophobic residues involved in the protein−lipid interactions of ACO with the bilayer were L21, V35, I60, F69, F334, and L475. A histidine and an asparagine (H155 and N340, respectively) also seem to play a role in membrane binding. The main basic residues in contact with the bilayer were R22, K66, and R454.

(v) P450. A combination of basic (R73, R197, H231, and R236) and hydrophobic (L43, I97, F220, F223, and F227) residues anchored P450 in the bilayer in the simulations. The results obtained are in agreement with the proposed membrane association mode (*41*).

Deep Insertion. (i) COX-1. In this case, H90:A, R97:B, W100:B, and W323:B were the key residues that aid stabilization of the foot in the bilayer. The residues involved in membrane binding were in agreement with previous computational studies, reported in the literature (*10*).

(ii) COX-2. The key interactions seen in the simulation involve residues R69:B, R77:B, P84:A, P86:B, H95:A, H95:B, R109:B, K114:A, and R469:B. All of these are located in the putative membrane binding region, the foot (*42*). The two residues that formed the most frequent interactions with phospholipids were L108:A and R77:B. Our results are in partial agreement with previous atomistic simulations (*10*), although COX-2 seems to insert more deeply into the bilayer in the CG-MD simulations. Significantly, both COX-1 and COX-2 appear to tilt in the bilayer, such that one of the monomers interacts with the bilayer far more than the other. This suggests there may be more than one mode of interaction of COX-2 with the bilayer.

(iii) SHC. The bacterial homologue of OSC, SHC (the two proteins share just 23% sequence identity) interacted in a different manner with the bilayer. It caused significant disruption to the hydrophobic core of the bilayer (see Discussion). It has previously been proposed that SHC interacts with the bilayer by inserting into the hydrophobic core of the bilayer (*43*). The suggested interaction residues

were L23, A52, F174, V182, D384, F442, and C443 which are relatively close to the active site (within 10 Å). We observed deep insertion of SHC in our simulations. F174, V182, F442, and C443 were key residues in terms of protein−lipid interactions in the simulations. Other residues contacting lipids included P236, F237, and V296. In addition, some deeply inserted basic residues (K274, R406, and K549) associated with phosphate moieties of the opposing leaflet of the bilayer, resulting in a degree of local perturbation of the bilayer structure (as discussed further below).

(iv) 11-β HSD1. The main hydrophobic residues forming contacts are M31, M57, I50, and F201. Other residues involved were P178 and E293. Also, a high percentage of contacts by lipids with basic residues were formed. Key basic residues were evenly distributed over the surface of the membrane binding domain, including R28, K35, R77, H87, K225, R252, and K294.

(v) CrAT. This protein has been proposed to contain a 30-amino acid region (205−234) which forms a putative membrane binding domain (*44*). Interestingly, we do not see any evidence in our simulations of this region interacting with the bilayer. Instead, we observe frequent interactions between the following hydrophobic residues and phospholipids: I203, V205, L525, and P535. We also observe the following basic residues interacting with phospholipid molecules: K186, K261, K268, K397, and R181. Furthermore, we also observe other polar residues (e.g., S189, Q526, and D540) interacting with the bilayer.

In summary, the predominant interactions with the bilayer observed in our simulations are either via basic residues (K, R, and to a lesser extent H) or via hydrophobic side chains (especially F, L, I, and V). This is broadly in agreement with an earlier structural bioinformatics analysis of five monotopic proteins which suggested basic residues and L, W, and Y played a key role in anchoring monotopic membrane proteins (*3*).

Local Bilayer Perturbation. In the preceding discussion, we have (provisionally) classified the monotopic proteins into two groups, on the basis of the predicted depth of insertion into the bilayer from the CG-MD simulations. Inspection of structures (Figure 5) and of density profiles along the bilayer normal (Figure 6) also provides evidence of local thinning of the bilayer by some of the more deeply inserting proteins. We have quantified such thinning and have explored the relationship between the type of residues involved in membrane binding and anchoring and the effect of these residues on bilayer structure. Our results suggest that the proportion of buried basic residues in contact with phospholipids is crucial in determining the effect of the protein on the bilayer.

The phosphate−phosphate distance (d_{PP}) in the direction of the bilayer normal (z) provides a convenient simple measure of bilayer thickness. This distance can be measured for lipids as a function of their distance from the protein (Figure 9A), indicating that perturbations are local and decay such that the bilayer thickness returns to its unperturbed value (d_{PP} = 39−40 Å) at a distance of ∼20 Å from the protein center of mass. Comparing different proteins indicates little perturbation of bilayer thickness for a "shallow insertion" protein (e.g., FAAH), whereas there is significant perturbation for a more deeply inserted protein [e.g., SHC (Figure 9A)]. Significantly, the degree of perturbation seems to correlate

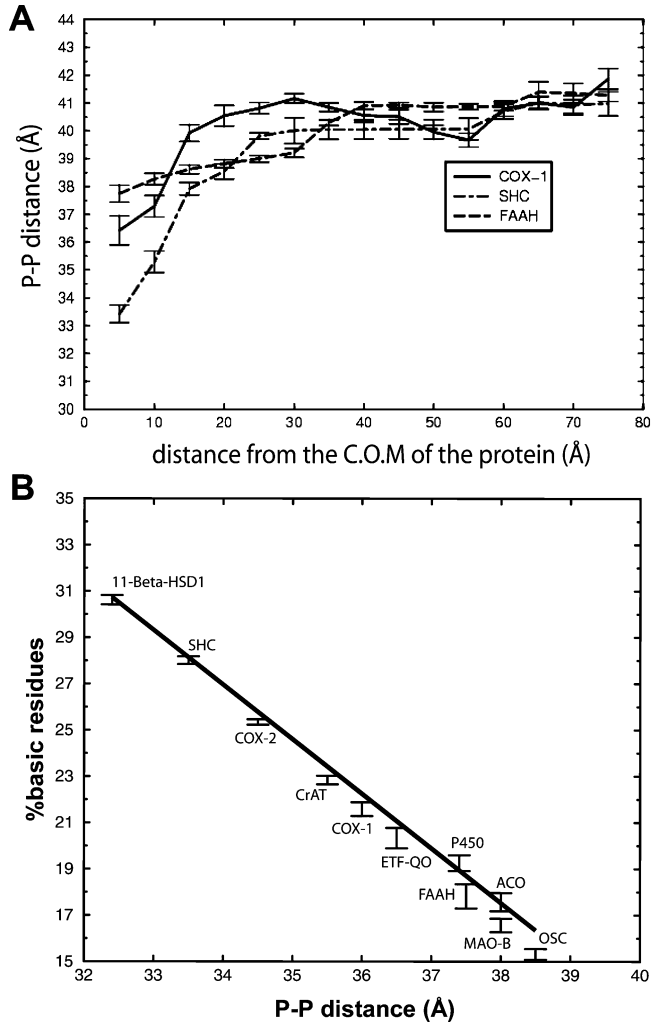

FIGURE 9: Local changes in bilayer thickness. (A) Time-averaged distance from 200 to 700 ns between a set of phosphate particles in the lower and upper leaflets of the bilayer as a function of the radial distance of these phosphates from the center of mass (COM) of the protein. (B) Relationship between the percentage of basic residues (in the region forming contacts with the lipids) and the phosphate−phosphate distance (at a radial distance of 5 Å from the COM of the protein). Error bars are standard deviations of three repeat trajectories for each system.

with the percentage of basic residues which are membrane-bound [i.e., the percentage of basic residues among those forming a contact with the lipids (Figure 9B)]. Thus, interactions of basic residues seem to play a key role in local bilayer distortions.

DISCUSSION

This study has demonstrated the utility of CG-MD simulations in predicting the orientation of complex monotopic membrane enzymes relative to a lipid bilayer and in revealing the interactions of such proteins with the lipid molecules. As such, it extends previous CG-MD simulations of membrane protein toxins (*21*) and of simpler monotopic enzymes [e.g., phospholipase A_2 (*22*)]. It also analyzes a greater range of monotopic enzymes over more extended simulation times than has been possible in atomistic simulations (*9*−*11*). For many of the proteins (e.g., OSC, FAAH, MAO-B, ACO, and ETF-QO), we have studied the predicted orientation and interactions with a bilayer agree

with those suggested previously on the basis of inspection of X-ray structures. For three other proteins (COX-1, COX-2, and CrAT), our predictions substantially modify earlier models. For two proteins (SHC and 11-β HSD1), our predictions differ from previous suggestions. The particulate nature of the CG-MD simulation means that residues forming frequent interactions with lipid molecules can readily be identified. Unfortunately, there are relatively few data from mutagenesis studies of putative membrane binding regions of monotopic enzymes. Studies of COX-1 and COX-2 suggested the membrane binding regions resided within residues 74−140 and 59−111, respectively (*45*). This is in good agreement with the results of our simulations of COX-1 and COX-2. This study also provided some insights into the difficulties involved in performing extensive mutagenesis studies on a membrane-associated segment of a monotopic protein, as the majority of their mutations were expressed as misfolded aggregates.

Although extensive mutagenesis and/or spectroscopic data on membrane anchors are not available for comparison, there is a detailed structural bioinformatics analysis (based on five monotopic proteins localized relative to a hydrophobic "slab" model of a bilayer) which suggested basic (K and R) and hydrophobic (especially L, W, and Y) residues played a key role in anchoring monotopic membrane proteins (*3*). In our simulations, the predominant interactions with the bilayer are either via basic residues (K, R, and to a lesser extent H) or via hydrophobic side chains (especially F, L, I, and V). Thus, simulations and structural bioinformatics approaches seem to be in agreement. It seems likely that the hydrophobic residues act as a "shield" for basic residues when inserting into a bilayer (i.e., the free energy of insertion of the basic residues is offset by the presence of hydrophobic residues).

Our results suggest that the monotopic enzymes may be broadly classified into two categories, on the basis of their interaction with the bilayer: (i) those which interact primarily with the bilayer surface (i.e., shallow insertors) and (ii) those which are inserted more deeply into the hydrophobic core of the bilayer, resulting in a significant degree of (local) perturbation of the bilayer. The latter class of proteins seem to act via hydrophobic patches that penetrate deeply into the bilayer, aided by basic residues that interact not only with the phosphate proximal leaflet but also, to a lesser extent, with phosphates in the opposing leaflet. The latter interaction is possible because of a shielding effect of the hydrophobic residues. Given the hydrophobic nature of many substrates and inhibitors of monotopic enzymes, it is tempting to speculate that such local perturbation may be of functional importance. Consequently, it would be of interest if such perturbations could be explored via a combination of mutational and spectroscopic studies.

This study has presented novel insights into the interactions of monotopic enzymes with simple lipid bilayer membranes. However, one should consider the possible shortcomings of a computational study of this nature. While CG-MD simulations provide access to longer time scales (by ~2 orders of magnitude) and hence sample system configurations more effectively than atomistic simulations, one must remain critically aware of the approximations intrinsic in the CG approach. For example, the electrostatic interactions are shifted and scaled by a relative dielectric of 20 to compensate for the absence of dipoles on the water particles. To explore the consequences of such approximations, we have previously validated our methodology for both integral membrane proteins (*6, 23*) and for (simpler) proteins binding at the membrane surface (*21, 22*). Furthermore, although there has been some discussion of the accuracy of the CG approach (*46*), comparison of the energetic cost of insertion of, for example, a single basic side chain within a hydrophobic α-helix into the center of a lipid bilayer in atomistic (*47*) and in CG (*48*) simulations suggests that even in this extreme test case, the CG method is in agreement within a factor of 2 with the corresponding atomistic simulations. Thus, for translating a polyleucine α-helix containing a single arginine residues along the bilayer normal, the energetic barrier at the center of the bilayer is ~29 kT by atomistic simulations and ~15 kT by CG simulations. For water/cyclohexane partition energies of neutral amino acid side chain analogues, the correlation between CH simulation and experimental values is as good ($r = 0.93$) as for comparable atomistic simulations (*48*). We have also shown that the results of this study are robust whether an earlier (*19*) or later (*48*) version of the CG force field (the versions differing in the polarity of the arginine side chain) is used. We has also explored the use of a modified version of the recent MARTINI CG force field (*20*) for, e.g., COX-2 and FAAH. Our preliminary analysis (of contact residues and of local bilayer thickness) does not indicate any major differences between the simulations run with our original force field and MARTINI, although there may be less distortion of the bilayer with MARTINI in the case of COX-2. This merits a more detailed examination in a future comparative study.

Another approximation used in this study is the use of an elastic network model to represent the tertiary structure of the protein (and also to compensate for non-protein, e.g., heme, atoms omitted from the CG representation). Simple ENMs seem to be able to reproduce the overall dynamics of proteins (*25, 49, 50*) to a level appropriate for the current study of protein−membrane interactions. However, it will be of interest to combine more complex network models (reviewed in, e.g., refs *51* and *52*) with the current CG approach.

The studies reported in this paper have all employed a self-assembly protocol to insert the protein optimally into a bilayer. A number of simulations were also performed with a preformed lipid bilayer, and the protein initially close to (but not inserted into) the bilayer surface. These simulations yielded results similar to those of the self-assembly simulations, although with lower extents of insertion. A further limitation of the current studies is the use of a single lipid (DPPC) model throughout. We did run simulations of MAO-B with a (relatively simple) mixed lipid (POPC/POPE) bilayer to facilitate comparison with the AT-MD simulation. Interestingly, we observe no significant difference in the bilayer orientation of the protein. However, more complex lipid compositions (e.g., inclusion of cholesterol) have yet to be investigated. Given that the phospholipid composition in a membrane in vivo may vary according to the subcellular location of a protein, the use of more complex mixtures of lipids will be a key extension of such simulation studies in the future. This will be facilitated by ongoing refinements in CG models and parameters (see, e.g., refs *20*, *53*, and *54*). A further possible refinement would be to analyze

protein−lipid interactions in terms of packing scores (*55*) to further calibrate the CG versus AT simulation approaches.

The CG-MD simulations presented here may also provide a starting point for multiscale simulations (*51, 52*). For example, a multiscale approach has been useful in exploring the deformation of planar lipid bilayers in the presence of multiple copies of the BAR domain protein (*56*). Preliminary results (K. Balali-Mood et al., unpublished data) suggest a multiscale approach starting from CG-MD self-assembly simulations can be used to explore the functionally important dynamics of monotopic enzymes such as FAAH.

ACKNOWLEDGMENT

Our thanks go out to our colleagues in the IntBioSim project and to Philip Biggin and Syma Khalid for helpful discussions.

SUPPORTING INFORMATION AVAILABLE

A table providing further details of basic and hydrophobic residues which form contacts with lipids. This material is available free of charge via the Internet at http://pubs.acs.org.

REFERENCES

1. Wallin, E., and von Heijne, G. (1998) Genome-wide analysis of integral membrane proteins from eubacterial, archean, and eukaryotic organisms. *Protein Sci. 7*, 1029–1038.
2. White, S. H. (2004) The progress of membrane protein structure determination. *Protein Sci. 13*, 1948–1949.
3. Granseth, E., von Heijne, G., and Elofsson, A. (2005) A study of the membrane-water interface region of membrane proteins. *J. Mol. Biol. 346*, 377–385.
4. Bracey, M. H., Cravatt, B. F., and Stevens, R. C. (2004) Structural commonalities among integral membrane enzymes. *FEBS Lett. 567*, 159–165.
5. Hunte, C., and Richers, S. (2008) Lipids and membrane protein structures. *Curr. Opin. Struct. Biol. 18*, 406–411.
6. Scott, K. A., Bond, P. J., Ivetac, A., Chetwynd, A. P., Khalid, S., and Sansom, M. S. P. (2008) Coarse-grained MD simulations of membrane protein-bilayer self-assembly. *Structure 16*, 621–630.
7. Chandrasekharan, N. V., and Simmons, D. L. (2004) The cyclooxygenases. *Genome Biol. 5*, 241.
8. Lindahl, E., and Sansom, M. S. P. (2008) Membrane proteins: Molecular dynamics simulations. *Curr. Opin. Struct. Biol. 18*, 425–431.
9. Nina, M., Bernèche, S., and Roux, B. (2000) Anchoring of a monotopic membrane protein: The binding of prostaglandin H2 synthase-1 to the surface of a phospholipid bilayer. *Eur. Biophys. J. 29*, 439–454.
10. Fowler, P. W., and Coveney, P. V. (2006) A computational protocol for the integration of the monotopic protein prostaglandin H2 synthase into a phospholipid bilayer. *Biophys. J. 91*, 401–410.
11. Fowler, P. W., Balali-Mood, K., Deol, S., Coveney, P. V., and Sansom, M. S. P. (2007) Monotopic enzymes and lipid bilayers: A comparative study. *Biochemistry 46*, 3108–3115.
12. Sapay, N., Guermeur, Y., and Deleage, G. (2006) Prediction of amphipathic in-plane membrane anchors in monotopic proteins using a SVM classifier. *BMC Bioinf.,* 7.
13. Lomize, A. L., Pogozheva, I. D., Lomize, M. A., and Mosberg, H. I. (2006) Positioning of proteins in membranes: A computational approach. *Protein Sci. 15*, 1318–1333.
14. Lomize, M. A., Lomize, A. L., Pogozheva, I. D., and Mosberg, H. I. (2006) OPM: Orientations of proteins in membranes database. *Bioinformatics 22*, 623–625.
15. Lomize, A. L., Pogozheva, I. D., Lomize, M. A., and Mosberg, H. I. (2007) The role of hydrophobic interactions in positioning of peripheral proteins in membranes. *BMC Struct. Biol.,* 7.
16. Marrink, S. J., de Vries, A. H., and Mark, A. E. (2004) Coarse grained model for semiquantitative lipid simulations. *J. Phys. Chem. B 108*, 750–760.
17. Shelley, J. C., Shelley, M. Y., Reeder, R. C., Bandyopadhyay, S., and Klein, M. L. (2001) A coarse grain model for phospholipid simulations. *J. Phys. Chem. B 105*, 4464–4470.
18. Venturoli, M., Smit, B., and Sperotto, M. M. (2005) Simulation studies of protein-induced bilayer deformations, and lipid-induced protein tilting, on a mesoscopic model for lipid bilayers with embedded proteins. *Biophys. J. 88*, 1778–1798.
19. Bond, P. J., and Sansom, M. S. P. (2006) Insertion and assembly of membrane proteins via simulation. *J. Am. Chem. Soc. 128*, 2697–2704.
20. Monticelli, L., Kandasamy, S. K., Periole, X., Larson, R. G., Tieleman, D. P., and Marrink, S. J. (2008) The MARTINI coarse grained force field: Extension to proteins. *J. Chem. Theory Comput. 4*, 819–834.
21. Wee, C. L., Bemporad, D., Sands, Z. A., Gavaghan, D., and Sansom, M. S. P. (2007) SGTx1, a Kv channel gating-modifier toxin, binds to the interfacial region of lipid bilayers. *Biophys. J. 92*, L07–L09.
22. Wee, C. L., Balali-Mood, K., Gavaghan, D., and Sansom, M. S. P. (2008) The interaction of phospholipase A2 with a phospholipid bilayer: Coarse-grained molecular dynamics simulations. *Biophys. J. 95*, 1649–1657.
23. Bond, P. J., Holyoake, J., Ivetac, A., Khalid, S., and Sansom, M. S. P. (2007) Coarse-grained molecular dynamics simulations of membrane proteins and peptides. *J. Struct. Biol. 157*, 593–605.
24. van der Spoel, D., Lindahl, E., Hess, B., Groenhof, G., Mark, A. E., and Berendsen, H. J. (2005) GROMACS: Fast, flexible, and free. *J. Comput. Chem. 26*, 1701–1718.
25. Atilgan, A. R., Durell, S. R., Jernigan, R. L., Demirel, M. C., Keskin, O., and Bahar, I. (2001) Anisotropy of fluctuation dynamics of proteins with an elastic network model. *Biophys. J. 80*, 505–515.
26. Berendsen, H. J. C., Postma, J. P. M., van Gunsteren, W. F., DiNola, A., and Haak, J. R. (1984) Molecular dynamics with coupling to an external bath. *J. Chem. Phys. 81*, 3684–3690.
27. van Gunsteren, W. F., Kruger, P., Billeter, S. R., Mark, A. E., Eising, A. A., Scott, W. R. P., Huneberger, P. H., and Tironi, I. G. (1996) *Biomolecular Simulation: The GROMOS96 Manual and User Guide*, Biomos & Hochschulverlag AG an der ETH Zurich, Zurich, Switzerland.
28. Darden, T., York, D., and Pedersen, L. (1993) Particle mesh Ewald: An N.log(N) method for Ewald sums in large systems. *J. Chem. Phys. 98*, 10089–10092.
29. Hess, B., Bekker, H., Berendsen, H. J. C., and Fraaije, J. G. E. M. (1997) LINCS: A linear constraint solver for molecular simulations. *J. Comput. Chem. 18*, 1463–1472.
30. Parrinello, M., and Rahman, A. (1981) Polymorphic transitions in single crystals: A new molecular-dynamics method. *J. Appl. Phys. 52*, 7182–7190.
31. Nose, S. (1984) A molecular dynamics method for simulations in the canonical ensemble. *Mol. Phys. 52*, 255–268.
32. Humphrey, W., Dalke, A., and Schulten, K. (1996) VMD: Visual Molecular Dynamics. *J. Mol. Graphics 14*, 33–38.
33. Psachoulia, E., Bond, P. J., Fowler, P. W., and Sansom, M. S. P. (2008) Helix-helix interactions in membrane proteins: Coarse grained simulations of glycophorin helix dimerization. *Biochemistry 47*, 10503–105012.
34. Gaboriaud, C., Juanhuix, J., Gruez, A., Lacroix, M., Darnault, C., Pignol, D., Verger, D., Fontecilla-Camps, J. C., and Arlaud, G. J. (2003) The crystal structure of the globular head of complement protein C1q provides a basis for its versatile recognition properties. *J. Biol. Chem. 278*, 46974–46982.
35. Eyal, E., Yang, L., and Bahar, I. (2006) Anisotropic Network Model: Systematic evaluation and a new web interface. *Bioinformatics 22*, 2619–2627.
36. Thoma, R., Schulz-Gasch, T., D'Arcy, B., Benz, J., Aebi, J., Dehmlow, H., Hennig, M., Stihle, M., and Ruf, A. (2004) Insight into steroid scaffold formation from the structure of human oxidosqualene cyclase. *Nature 432*, 118–122.
37. Bracey, M. H., Hanson, M. A., Masuda, K. R., Stevens, R. C., and Cravatt, B. F. (2002) Structural adaptations in a membrane enzyme that terminates endocannabinoid signaling. *Science 298*, 1793–1796.
38. Zhang, J., Frerman, F. E., and Kim, J. J. (2006) Structure of electron transfer flavoprotein-ubiquinone oxidoreductase and electron transfer to the mitochondrial ubiquinone pool. *Proc. Natl. Acad. Sci. U.S.A. 103*, 16212–16217.
39. Ruf, A., Muller, F., D'Arcy, B., Stihle, M., Kusznir, E., Handschin, C., Morand, O. H., and Thoma, R. (2004) The monotopic

membrane protein human oxidosqualene cyclase is active as monomer. *Biochem. Biophys. Res. Commun. 315*, 247–254.
40. Kloer, D. P., Ruch, S., Al-Babili, S., Beyer, P., and Schulz, G. E. (2005) The structure of a retinal-forming carotenoid oxygenase. *Science 308*, 267–269.
41. Zhao, Y., White, M. A., Muralidhara, B. K., Sun, L., Halpert, J. R., and Stout, C. D. (2006) Structure of microsomal cytochrome P450 2B4 complexed with the antifungal drug bifonazole: Insight into P450 conformational plasticity and membrane interaction. *J. Biol. Chem. 281*, 5973–5981.
42. Kiefer, J. R., Pawlitz, J. L., Moreland, K. T., Stegeman, R. A., Hood, W. F., Gierse, J. K., Stevens, A. M., Goodwin, D. C., Rowlinson, S. W., Marnett, L. J., Stallings, W. C., and Kurumbail, R. G. (2000) Structural insights into the stereochemistry of the cyclooxygenase reaction. *Nature 405*, 97–101.
43. Wendt, K. U., Lenhart, A., and Schulz, G. E. (1999) The structure of the membrane protein squalene-hopene cyclase at 2.0 Å resolution. *J. Mol. Biol. 286*, 175–187.
44. Rufer, A. C., Thoma, R., Benz, J., Stihle, M., Gsell, B., De Roo, E., Banner, D. W., Mueller, F., Chomienne, O., and Hennig, M. (2006) The crystal structure of carnitine palmitoyltransferase 2 and implications for diabetes treatment. *Structure 14*, 713–723.
45. Spencer, A. G., Thuresson, E., Otto, J. C., Song, I., Smith, T., DeWitt, D. L., Garavito, R. M., and Smith, W. L. (1999) The membrane binding domains of prostaglandin endoperoxide H synthases 1 and 2. Peptide mapping and mutational analysis. *J. Biol. Chem. 274*, 32936–32942.
46. Vorobyov, I., Li, L., and Allen, T. W. (2008) Assessing atomistic and coarse-grained force fields for protein-lipid interactions: The formidable challenge of an ionizable side chain in a membrane. *J. Phys. Chem. B 112*, 9588–9602.
47. Dorairaj, S., and Allen, T. W. (2007) On the thermodynamic stability of a charged arginine side chain in a transmembrane helix. *Proc. Natl. Acad. Sci. U.S.A. 104*, 4943–4948.
48. Bond, P. J., Wee, C. L., and Sansom, M. S. P. (2008) Coarse-grained molecular dynamics simulations of the energetics of helix insertion into a lipid bilayer. *Biochemistry 47*, 11321–11331.
49. Keskin, O., Jernigan, R. L., and Bahar, I. (2000) Proteins with similar architecture exhibit similar large-scale dynamic behavior. *Biophys. J. 78*, 2093–2106.
50. Yang, L. W., Liu, X., Jursa, C. J., Holliman, M., Rader, A. J., Karimi, H. A., and Bahar, I. (2005) iGNM: A database of protein functional motions based on Gaussian Network Model. *Bioinformatics 21*, 2978–2987.
51. Ayton, G. A., Noid, W. G., and Voth, G. A. (2007) Multiscale modeling of biomolecular systems: In serial and in parallel. *Curr. Opin. Struct. Biol. 17*, 192–198.
52. Sherwood, P., Brooks, B. R., and Sansom, M. S. P. (2008) Multiscale methods for macromolecular simulations. *Curr. Opin. Struct. Biol. 18*, 630–640.
53. Marrink, S. J., Risselada, J., Yefimov, S., Tieleman, D. P., and de Vries, A. H. (2007) The MARTINI forcefield: Coarse grained model for biomolecular simulations. *J. Phys. Chem. B 111*, 7812–7824.
54. Marrink, S. J., de Vries, A. H., and Tieleman, D. P. (2008) Lipids on the move: Simulations of membrane pores, domains, stalks and curves. *Biochim. Biophys. Acta,* doi: 10.1016/j.bbamem.2008.10.006.
55. Grossfield, A., Feller, S. E., and Pitman, M. C. (2006) A role for direct interactions in the modulation of rhodopsin by ω-3 polyunsaturated lipids. *Proc. Natl. Acad. Sci. U.S.A. 103*, 4888–4893.
56. Arkhipov, A., Yin, Y., and Schulten, K. (2008) Four-scale description of membrane sculpting by BAR domains. *Biophys. J. 95*, 2806–2821.
57. Ogg, D., Elleby, B., Norstrom, C., Stefansson, K., Abrahmsen, L., Oppermann, U., and Svensson, S. (2005) The crystal structure of guinea pig 11β-hydroxysteroid dehydrogenase type 1 provides a model for enzyme-lipid bilayer interactions. *J. Biol. Chem. 280*, 3789–3794.
58. Gupta, K., Selinsky, B. S., Kaub, C. J., Katz, A. K., and Loll, P. J. (2004) The 2.0 Å resolution crystal structure of prostaglandin H(2) synthase-1: Structural insights into an unusual peroxidase. *J. Mol. Biol. 335*, 503–518.
59. Hsiao, Y.-S., Jogl, G., and Tong, L. (2004) Structural and biochemical studies of the substrate selectivity of carnitine acetyltransferase. *J. Biol. Chem. 279*, 31584–31589.
60. Binda, C., Li, M., Hubalek, F., Restelli, N., Edmondson, D. E., and Mattevi, A. (2003) Insights into the mode of inhibition of human mitochondrial monoamine oxidase B from high-resolution crystal structures. *Proc. Natl. Acad. Sci. U.S.A. 100*, 9750–9755.

BI8017398